JGR Space Physics

RESEARCH ARTICLE
10.1029/2024JA033208

A Multi-Platform Statistical Analysis of the Azimuthal Spatial Extent of the Microburst Precipitation Region

S. S. Elliott[1], C. Colpitts[1], A. W. Breneman[2], J. M. Pettit[2], K. A. Cantwell[3], C. A. Cattell[1], A. J. Halford[2], M. Shumko[4], J. Sample[5], A. Johnson[5], Y. Miyoshi[6], Y. Kasahara[7], R. N. Troyer[8], R. Millan[3], T. Hori[6], I. Shinohara[9], S. Matsuda[7], and A. Matsuoka[7]

[1]The University of Minnesota, Minneapolis, MN, USA, [2]NASA Goddard Space Flight Center, Greenbelt, MD, USA, [3]Dartmouth College, Hanover, NH, USA, [4]Johns Hopkins University Applied Physics Laboratory, Laurel, MD, USA, [5]Montana State University, Bozeman, MT, USA, [6]ISSEE, Nagoya University, Nagoya, Japan, [7]Kanazawa University, Kanazawa, Japan, [8]Space Dynamics Laboratory, North Logan, UT, USA, [9]ISAS/JAXA, Sagamihara, Japan

Key Points:

- We perform a statistical analysis of chorus and energetic electron precipitation to constrain the spatial extent of the precipitation region
- Results suggest microbursts may frequently constitute a source of electron loss from the outer radiation belt
- The azimuthal extent increases with geomagnetic activity

Correspondence to:
S. S. Elliott,
tetri006@umn.edu

Citation:
Elliott, S. S., Colpitts, C., Breneman, A. W., Pettit, J. M., Cantwell, K. A., Cattell, C. A., et al. (2024). A multi-platform statistical analysis of the azimuthal spatial extent of the microburst precipitation region. *Journal of Geophysical Research: Space Physics*, *129*, e2024JA033208. https://doi.org/10.1029/2024JA033208

Received 21 AUG 2024
Accepted 19 NOV 2024

Abstract Microbursts are impulsive injections of energetic (few keV to >MeV) electrons into the atmosphere, primarily caused by nonlinear scattering driven by whistler mode chorus waves. While the relative importance of microburst precipitation as a loss process has not been fully quantified, many studies have shown microbursts may play a significant role in the loss of outer radiation belt electrons. We present a multi-platform statistical analysis of chorus and energetic electron precipitation in an attempt to constrain the azimuthal spatial extent (ΔMLT) of the microburst precipitation region and determine how this extent varies with geomagnetic activity. Statistical upper bounds of this azimuthal extent are determined with observations of general energetic electron precipitation that can include direct microburst detections, while statistical lower bounds determination requires direct microburst detections. The resulting distributions of both upper and lower bounds azimuthal extent suggest that microbursts may frequently constitute an important source of electron loss from the outer radiation belt. We find that 36% of upper bound events in the dawn sector span more than 5 hr in MLT. This azimuthal extent increases with geomagnetic activity, particularly in the dawn and noon MLT sectors.

Plain Language Summary Microbursts are short-duration (<1 s) bursts of electrons that precipitate from the magnetosphere into the atmosphere. They are thought to be caused by scattering by a plasma wave called chorus. Microburst precipitation contributes to outer radiation belt loss after enhancements during geomagnetic storms. The contribution depends on the size and duration of the microburst region. We present a statistical analysis of chorus and energetic electron precipitation to determine the size of the microburst precipitation region. We also analyze how the size depends on geomagnetic activity. Our results show that the region is often large and the size increases with geomagnetic activity.

1. Introduction and Background

Earth's radiation belts are highly dynamic, and many competing processes contribute to their formation and depletion (see reviews by Thorne (2010), Millan and Thorne (2007), Ripoll et al. (2020), and Kanekal and Miyoshi (2021)). Quantifying electron precipitation into the atmosphere is critical for understanding these dynamics. Electron microbursts are short-duration (<1 s) precipitation events of energetic (few keV to >MeV) electrons into the atmosphere, first observed via balloon measurements (K. A. Anderson & Milton, 1964), and subsequently on satellites (e.g., Blake et al., 1996; Imhof & Nightingale, 1992) and balloons (e.g., Millan et al., 2002; Woodger et al., 2015). Observations suggest that microbursts can be an important loss mechanism in the outer radiation belt during storm main and early recovery phases (Lorentzen, Blake, et al., 2001; Lorentzen, Looper, & Blake, 2001; Millan & Thorne, 2007; O'Brien et al., 2004; Thorne et al., 2005; Tsurutani et al., 2013). Additionally, higher energy microbursts can deposit their energy at altitudes of the mesosphere or stratosphere (Marshall & Cully, 2020; Miyoshi et al., 2015, 2021), impacting magnetosphere-ionosphere-atmosphere coupling (see Seppälä et al. (2018) and references therein). Although microbursts have been observed for years, many questions remain regarding the physics of underlying scattering mechanisms and their relative importance in outer belt energetic electron loss (Blum & Breneman, 2020; Breneman et al., 2017; Douma et al., 2019).

Whistler mode chorus waves are generally believed to be the primary driver of electron microburst precipitation. Studies by Lorentzen, Blake, et al. (2001), Lorentzen, Looper, and Blake (2001), and Douma et al. (2017) have shown similarities in temporal (Douma et al., 2019; Nakamura et al., 2000; X.-J. Zhang et al., 2022) and spatial

(MLT, *L*) occurrence of chorus and microbursts (e.g., Li et al., 2009). Theoretical and observational studies (e.g., Agapitov et al., 2017; Breneman et al., 2017; Douma et al., 2017; Lorentzen, Blake, et al., 2001; Mozer et al., 2018) suggest that microbursts are primarily caused by first order gyro resonant scattering by chorus waves. The resonant energy rapidly increases with background magnetic field strength such that lower energy microbursts (10s keV) are precipitated near the magnetic equator by locally generated chorus, while relativistic microbursts (>100s keV) are generated at higher magnetic latitudes by chorus that has propagated away from its near-equatorial source (Breneman et al., 2017; Chen et al., 2021; Colpitts et al., 2020; Horne et al., 2003; Kang et al., 2024; Kersten et al., 2011; Lorentzen, Blake, et al., 2001; Lorentzen, Looper, & Blake, 2001; Miyoshi et al., 2020; Nakamura et al., 2000; Namekawa et al., 2023; Saito et al., 2012; Shumko et al., 2023; Thorne et al., 2005).

It should be noted that there are several plasma waves and mechanisms efficient at energetic electron precipitation. Electromagnetic Ion Cyclotron (EMIC) waves can deplete the outer radiation belt of ∼MeV electrons (Blum et al., 2020; Capannolo et al., 2018; Drozdov et al., 2019, 2020; Shprits et al., 2017; Xiang et al., 2017; X.-J. Zhang et al., 2016). Therefore relativistic (>1 MeV) electron precipitation has been attributed to EMIC waves (Engebretson et al., 2008; Qin et al., 2020; Woodger et al., 2018; Yuan et al., 2018). However, EMIC waves can also precipitate electrons down to hundreds of keV, but the process is much less efficient and mainly occurs in the noon to post-midnight MLT sector (see Capannolo et al. (2023, 2019), Carson et al. (2012), Shekhar et al. (2017, 2018), Blum, Li, and Denton (2015), Blum, Halford, et al. (2015), and Woodger et al. (2018)). Other waves such as plasmaspheric hiss and ultralow frequency waves and mechanisms like current sheet scattering (CSS) can cause energetic electron precipitation, however these are likely not representative of the precipitation observed in this study due to their location and electron precipitation energy (i.e., plasmaspheric hiss is known to precipitate electrons within the plasmasphere, which is excluded from our study, CSS results in precipitation on the nightside at high L shells, and as mentioned, EMIC waves are most efficient at MeV energies, (see Capannolo et al. (2021, 2022) and Ma et al. (2020) and references therein). A review on the many processes that contribute to precipitation of outer radiation belt electrons can be found in Ripoll et al. (2020).

Overall, energetic electron precipitation is important for understanding the dynamic coupling between the magnetosphere, ionosphere, and atmosphere (see Pettit et al. (2023) and references therein). However, the relative importance of microburst precipitation as a source of electron loss from the outer radiation belt is still an open question. In order to fully answer this question, one needs an accurate measurement of the typical microburst flux (#/cm^2/sec) along with the spatial size of a microburst precipitation region. Ultimately, it is critical to quantify the loss rate due to microburst precipitation, and a necessary step is to determine the size and duration of microburst regions. This paper focuses on the azimuthal spatial size.

Recent studies (Breneman et al., 2017; Elliott, Breneman, Colpitts, Pettit, et al., 2022) have utilized a combination of high-altitude chorus wave observations from the Van Allen Probes (RBSP) and low-altitude microburst observations from the twin Focused Investigations of Relativistic Electron Burst: Intensity, Range, and Dynamics (FIREBIRD II) CubeSats (Crew et al., 2016; Spence et al., 2012) to constrain the size and duration of microburst regions. B. R. Anderson et al. (2017) used observations from the Balloon Array for Radiation belt Relativistic Electron Losses (BARREL) mission, FIREBIRD II, and AeroCube-6 (AC6) and found the region extended over 5 *L* and 4 hr MLT, but the authors noted that this was a likely underestimation due to a lack of MLT coverage. An earlier study by Lorentzen, Looper, and Blake (2001) analyzed an October 1998 storm using Solar, Anomalous, Magnetospheric Particles Explorer satellite data and found the microburst region to persist for 6 hr. They then used an estimation of 6 hr in MLT and 2 *L* based on previous observations (i.e., Lorentzen, Blake, et al., 2001; Nakamura et al., 2000) that showed microburst precipitation peaks at *L* of 4–6 in the morning sector between 3 and 8 MLT. Elliott, Breneman, Colpitts, Pettit, et al. (2022) presented a single event study that combined multiple observations of chorus and microburst precipitation to constrain the size of the microburst region. In that study, the *L* and MLT extent of the chorus (waves from RBSP, Arase, and ground-based VLF stations) and precipitation/microbursts (bounce loss cone (BLC) electron flux from the Polar Operational Environmental Satellites (POES) satellites combined with microbursts from FIREBIRD II and AC6 cubesats) were analyzed for three 9-hr time periods with continuous wave and precipitation activity. They estimated upper and lower bounds on the size of the regions for the three time periods. The lower bound was based on the overlap between chorus wave and microburst/precipitation observations. The upper bound was estimated by extending the region to areas where microburst/precipitation were observed, but no chorus due to lack of spacecraft coverage. In this study, we extend the results of Elliott, Breneman, Colpitts, Pettit, et al. (2022) across events from 2014 through 2019 to statistically

constrain the azimuthal spatial extent (ΔMLT) of a microburst precipitation region and determine how this extent depends on geomagnetic activity.

2. Instrumentation and Data Sets

This study includes a combination of measurements from 2014 to 2019 across several different platforms: chorus wave observations from Van Allen Probes (RBSP) (covering 2014–2019) (Mauk et al., 2013) and Arase (ERG) (2017–2019) (Miyoshi, Shinohara, et al., 2018), low Earth orbit (LEO) microburst observations from the FIREBIRD II (2015–2019) (Klumpar et al., 2015) and Aerospace Corporation AeroCube-6 (AC6) CubeSat missions (2015–2017), particle flux measurements from the POES (including the National Oceanic and Atmospheric Administration and Meteorological Operational satellites, NOAA/MetOp) (Evans & Greer, 2004; Rodger et al., 2010), and balloon-based X-ray measurements from the BARREL mission (Millan et al., 2013). These data were used in composite to constrain the azimuthal spatial extent of microburst-producing chorus regions.

2.1. Chorus Measurements

Chorus wave measurements were obtained from the Van Allen Probes (RBSP A, B) and Arase. RBSP was in a near-equatorial elliptical orbit ranging from ∼600 km to 5.8 Earth Radii (R_E). Because of the magnetic inclination, magnetic latitudes of up to 20° and L values up to $L > 6$ were sampled. Arase has an elliptical orbit ranging from 400 to 32,000 km, and inclination of 31° MLAT, sampling L values up to ∼10 (Miyoshi, Hori, et al., 2018).

Chorus waves on RBSP were identified using the Electric and Magnetic Field Instrument Suite and Integrated Science EMFISIS (Kletzing et al., 2013) magnetic field power spectral density (PSD) data. For this study, a threshold parameter was set such that the maximum PSD measurements within the frequency range of lower band chorus must be greater than 10^−7 nT^2/Hz (Hartley et al., 2019). Additionally, to encompass the entire outer radiation belt, a criterion was placed on orbit times when the spacecraft was within 3–7 L and up to 20° MLAT at all MLTs. In order for the waves to be identified as chorus, the spacecraft was required to be located outside the plasmasphere (i.e., density values from EMFISIS below 10*(6.6/L)^4 or 30 cm^3, whichever is smaller, see Bingham et al. (2018), Hartley et al. (2015, 2016), and Li et al. (2014)) and both the polarization and ellipticity were required to be greater than 0.5 (e.g., Santolík et al., 2002). Chorus waves on Arase were identified from one second resolution spectra from its Onboard Frequency Analyzer (OFA), a part of the Plasma Wave Experiment (PWE) instrument suite (Kasaba et al., 2017; Kasahara et al., 2018; Matsuda et al., 2018; Ozaki et al., 2018) with the Magnetic Field Experiment (MGF) (Matsuoka, Teramoto, Nomura, et al., 2018).

2.2. Microburst, Particle Flux, and Bremsstrahlung Measurements

Electron microburst measurements were obtained from the FIREBIRD II and AC6 CubeSats. FIREBIRD II, launched in 2015 with an orbit of 632 km by 433 km at 99.1° inclination, consisted of twin CubeSats, Flight Units 3 and 4 (FU3 and FU4), which measured energetic electrons from ∼250 to 1,000 keV in five differential energy channels and one integral (>1 MeV) channel (Crew et al., 2016; Klumpar et al., 2015; Spence et al., 2012). To detect microbursts, high resolution data (<=50 msec sampling) from the lowest differential energy channel of each collimated detector (230–300 keV on FU3 and 219–283 keV on FU4, Johnson et al., 2020) were used. In 2014 the AC6 CubeSats were launched into a LEO of 620 km by 700 km at 98° inclination, each with three radiation dosimeters. The current study uses the >35 keV dosimeter for electrons, which resolves microbursts by operating in a 10 Hz burst mode. An automated detection method (O'Brien et al., 2003; Shumko et al., 2020) was used to identify microbursts on FIREBIRD and AC6.

Electron flux measurements from the Medium Energy Proton and Electron Detector (MEPED) instruments on the POES satellites (NOAA15, NOAA18, NOAA19, METOP01, and METOP02) were used as a measure of strong electron flux in the BLC. Although POES measurements do not have the temporal resolution to distinguish between microburst precipitation and non-bursty precipitation, BLC flux increases may be indications of chorus wave driven precipitation (e.g., Bortnik & Thorne, 2007; Li et al., 2013). POES has excellent spatial coverage, providing important statistics for the current analysis, despite the limitations of low time resolution. We investigated the possibility that the higher resolution POES data (2-s) observed higher count rates during periods of chorus wave activity that perhaps were averaged out in the lower resolution (16-s) data used for this study. There was some indication of more "bursty" precipitation which overlapped with regions of strong chorus wave activity. Therefore, using the downsampled 16-s data may have resulted in an underestimation of precipitating flux from

Table 1
Types of Precipitation and Associated Upper/Lower Bounds

	Requires co-located chorus	Does not require chorus
Direct microburst observations and/or general precipitation from POES	Type 1 lower bound	Type 1 upper bound
Direct microburst observations only	Type 2 lower bound	Type 2 upper bound

Note. Type 1 precipitation combines POES and microbursts, while Type 2 precipitation only includes direct microburst precipitation. Upper bounds for both types do not require chorus observations, while lower bounds require the precipitation type and chorus to be observed.

POES. However, a more thorough statistical analysis of the higher resolution data is warranted, but beyond the scope of the current study.

Since POES BLC flux may or may not represent microburst precipitation, we perform our analysis both with and without the POES precipitation included. Precipitation that includes POES will subsequently be called Type 1 precipitation and precipitation that excludes POES (i.e., only direct microbursts) will be called Type 2 (see Table 1). For the analyses that include POES (Type 1 precipitation), we used the MEPED Precipitating Electron (MPE) data set, described in Pettit et al. (2021), which provides BLC flux for 27 energy channels from 27 keV to 8.9 MeV. We selected BLC fluxes from 84.7 to 320.8 keV to be consistent with the lowest FIREBIRD energy bin. These are also energies above auroral electrons, associated with microburst precipitation (e.g., Chen et al., 2022; Drozdov et al., 2020; Li et al., 2013 and references therein). We also removed times of low flux as described by Elliott, Breneman, Colpitts, Pettit, et al. (2022). We are aware that care must be taken with using MEPED electron data to compute precipitating electron flux due to the angular response function of the instrument, which can sometimes include trapped electrons (see Selesnick et al. (2020)). However, the angular response function issues only occur at times where there is little to no geomagnetic activity and at large MLTs outside the peak of the chorus wave distributions found in the current study.

Bremsstrahlung X-ray measurements (produced from collisions of precipitating electrons with atmospheric neutrals) were provided by BARREL. In total, 58 balloons launched during multiple campaigns between 2013 and 2020 collected X-ray data (via a sodium-iodide scintillator) in both hemispheres (Woodger et al., 2015). From 2014–2019, there were 35 balloons for which data were processed for scientific use, from which we used the first three energy channels (~25–180 keV) of the 50 ms resolution data. Microbursts were detected automatically based on the methods described in Cantwell and Millan (2024).

3. Methodology

To constrain the size of microburst-producing chorus regions, we identified all chorus and precipitation events across the platforms listed above from 2014 through 2019. We defined event intervals by the orbit of RBSP-A using the ephemeris start/stop times. These are roughly 9 hr in duration which provides sufficient spatial and temporal coverage for each event (see Elliott, Breneman, Colpitts, Pettit, et al. (2022)). This choice of interval may result in events that include multiple separate instances of microburst precipitation, which likely occur on the substorm timescales of 2–3 hr (Huang, 2005) or chorus decay timescales of ~1–2 hr (Troyer et al., 2024), but allows for the best estimate possible with the available data sets. Positive detections of chorus and precipitation were binned by MLT (1-hr bins) and L (2 L bins). Figure 1 shows an example event, where Figure 1a shows the chorus and precipitation observations, and Figure 1b shows the resulting binned data (1-hr MLT bins and 2 L bins) of microbursts from FIREBIRD, AC6, and BARREL, BLC flux precipitation from POES, and chorus waves from RBSP and Arase.

Figure 2 shows lower and upper bounds on the region size for Type 1 (Figures 2a and 2b, respectively) and Type 2 (Figures 2c and 2d, respectively) precipitation. It should be noted that we are only estimating the MLT extent of the region and therefore all L values (within 3–8 L) are included in each event.

In general, for each event, there is far less chorus coverage than there is combined coverage of POES precipitation and microbursts (Type 1 precipitation). Thus, we provide an upper bound of the energetic electron precipitation region based on the more comprehensive Type 1 precipitation coverage because we cannot know if chorus is active throughout this entire region (see Table 1). By contrast, by requiring both chorus and Type 1 precipitation to be observed we define a lower bound (i.e., region size minimum). This is a lower bound because the lack of

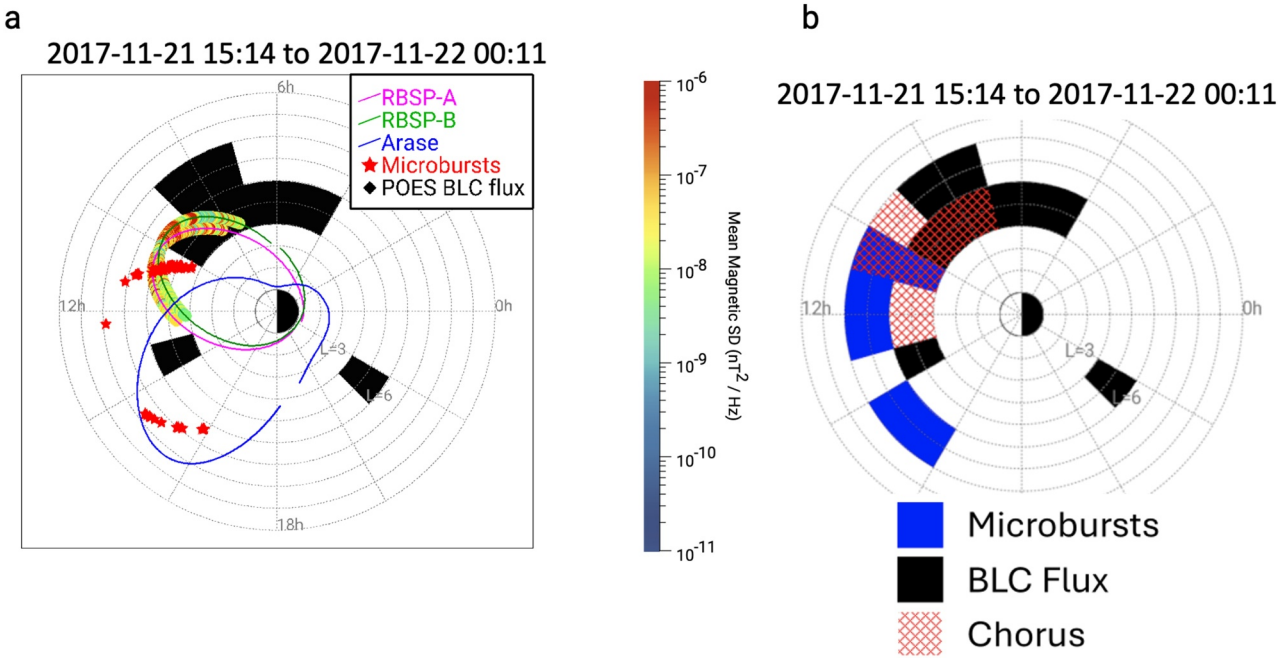

Figure 1. Example event showing multi-instrument observations of chorus and microburst/precipitation (left) and the resulting binned precipitation region (right). Panel (a) shows the MLT and *L* h locations of RBSP A and B (purple and green lines, respectively) and Arase (blue line). The rainbow color bar shows the mean magnetic spectral density of the lower-band chorus waves (between 0.1 and 0.5 Fce) observed. The blacked-out regions indicate where Polar Operational Environmental Satellites (POES) observes strong electron precipitation and the red stars indicate microburst observations from FIREBIRD, AC6, or Balloon Array for Radiation belt Relativistic Electron Losses. The data is then binned into 1-hr MLT bins and 2 *L* bins (b), where microburst precipitation observations are shown by the blue regions, strong bounce loss cone flux precipitation from POES regions are shown by the black regions, and chorus wave observations are shown by the red hashed regions.

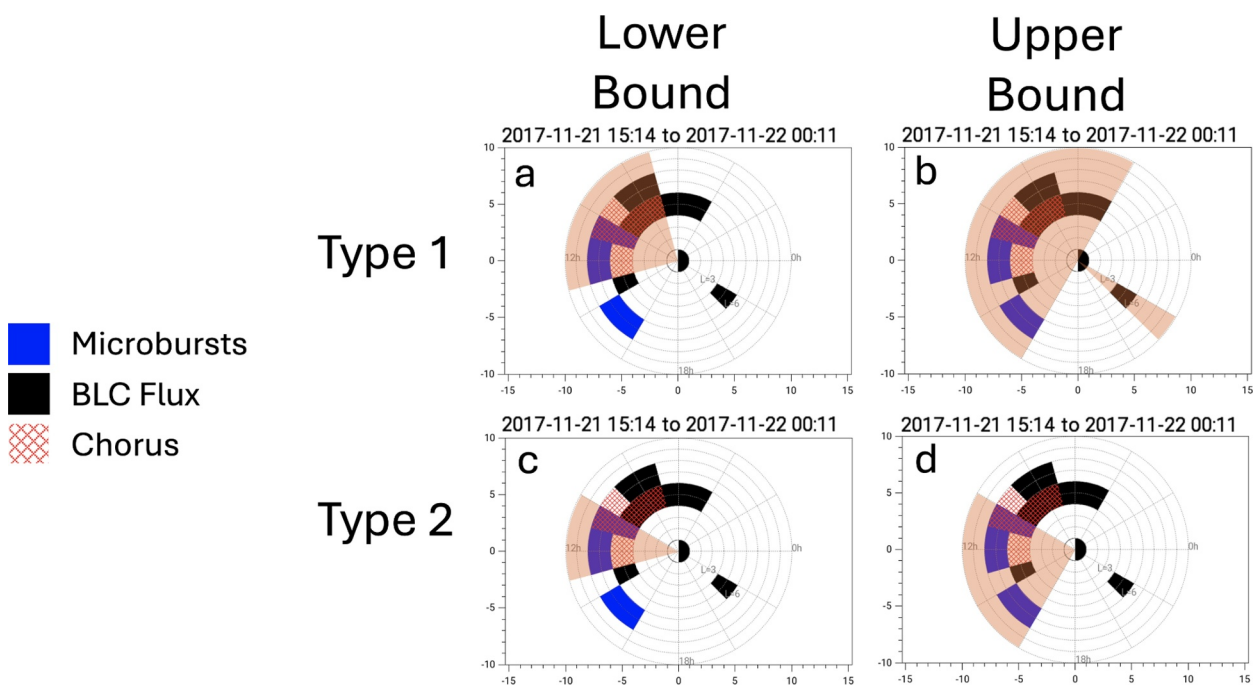

Figure 2. Data from Figure 1 binned into 1-hr MLT bins and 2 *L* bins (same method as Figure 1b). Panels (a, b) show the (a) lower and (b) upper bounds on the region size for Type 1 (microburst and Polar Operational Environmental Satellites bounce loss cone flux precipitation observations combined). Panels (c, d) show the (c) lower and (d) upper bounds on the region size for Type 2 (direct microburst observations only). The lower bound is defined as overlap between chorus and precipitation type. The upper bound is defined as all regions where (b) Type 1 or (d) Type 2 precipitation are observed. Note that *L* values are combined.

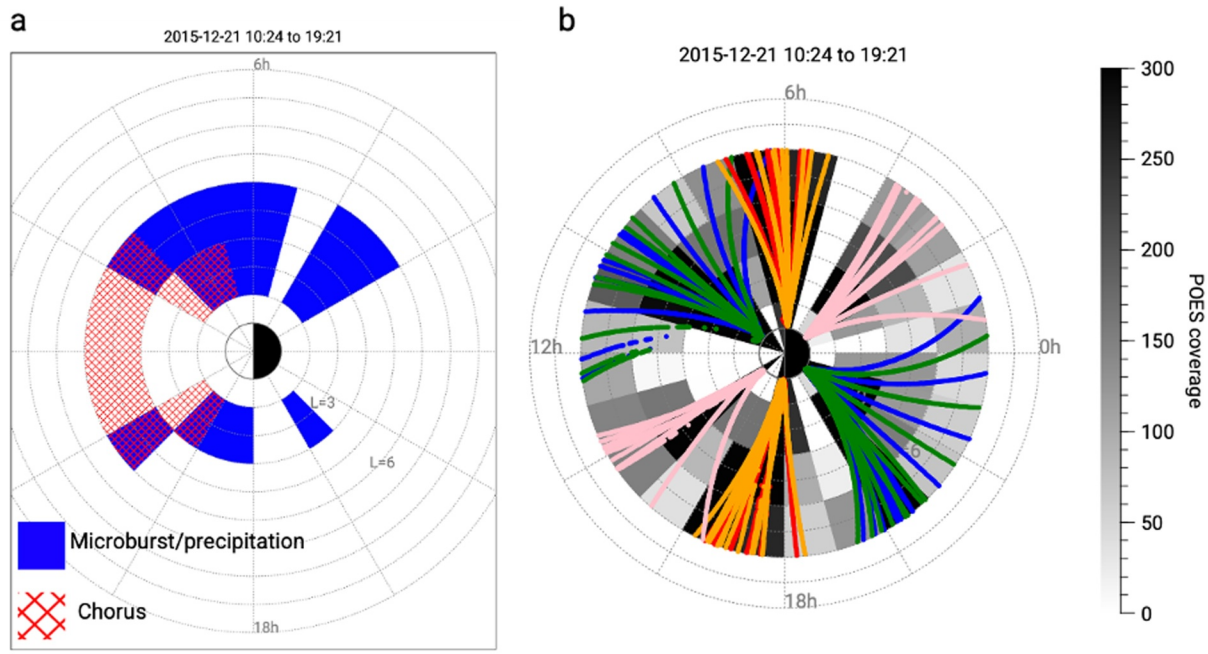

Figure 3. (a) Example chorus and microburst/precipitation observations binned plot for an event where Polar Operational Environmental Satellites (POES) has limited spatial coverage between 10 and 14 MLT. (b) POES coverage (gray scale) and POES instrument locations during the example event (each colored line represents a different POES satellite). This data gap between 10 and 14 MLT exists in the years after the Medium Energy Proton and Electron Detector instrument aboard NOAA16 was no longer in operation (2015 onwards). Other smaller data gaps exist at variable MLT (e.g., between 4 and 5 MLT in this case), which are remedied by our interpolation method.

chorus coverage means that the actual chorus region is likely larger than we observe. It should be noted that although POES provides the best spatial coverage of all the platforms listed above, POES does not have complete coverage (an example of which is shown in Figure 3b). However, these spatial gaps are smaller in delta-MLT than that of our spatial binning (with the exception of a consistent data gap around noon MLT and orbit-caused smaller gaps, which are discussed in detail below). It is possible that our threshold for selecting strong BLC flux may be too restrictive, resulting in missed precipitation regions. Because of this, the upper bound for Type 1 precipitation may not represent the maximum possible size of the region.

From examination of Figure 1a, it is evident that POES provides valuable additional observations in regions where the CubeSats and/or balloons are unable to provide measurements due to their limited coverage. However, because POES cannot detect microbursts, we repeat the upper and lower bound analyses, excluding POES precipitation and only including direct microburst detections (Type 2 precipitation, see Figures 2c and 2d). For Type 2 precipitation statistics, the upper bound is defined as the entire region where microbursts are detected. The lower bound requires both chorus and microbursts to be observed (see Table 1).

It is important to note that while the spatial coverage of POES is quite good, a significant gap exists in the noon MLT sector for the 2014–2019 data used here (Elliott, Breneman, Colpitts, Pettit, et al., 2022; Pettit et al., 2021). Figure 3 shows an example of the 1 hr MLT binned data for one event (Figure 3a for Type 1 precipitation) and the corresponding POES coverage (Figure 3b). A few clear data gaps can be identified, specifically around ∼10–14 MLT (a consistent data gap around noon MLT), 4–5 MLT, and 19–20 MLT (orbit-caused smaller data gaps). To deal with these two types of data gaps, we interpolate across the binned POES precipitation data for statistics that include POES (i.e., Type 1 precipitation). All gaps less than two bins wide (with a 1-hr MLT bin size) that have precipitation on both sides are interpolated across. Additionally, in the noon (10–14 MLT) sector we interpolate across gaps up to 4 bins wide based on the established method from Pettit et al. (2021). Figure 4 shows an example of the upper (Figure 4a) and lower (Figure 4b) bounds for Type 1 precipitation using the interpolation method described. It should be noted that within each ∼9 hr window there are sometimes a few POES passes in the 10–14 MLT sector (as shown in Figure 3b). However, since the data are sparse, they may not be representative of the entire time period, which could result in a misinterpretation of precipitation over these sectors. Because of

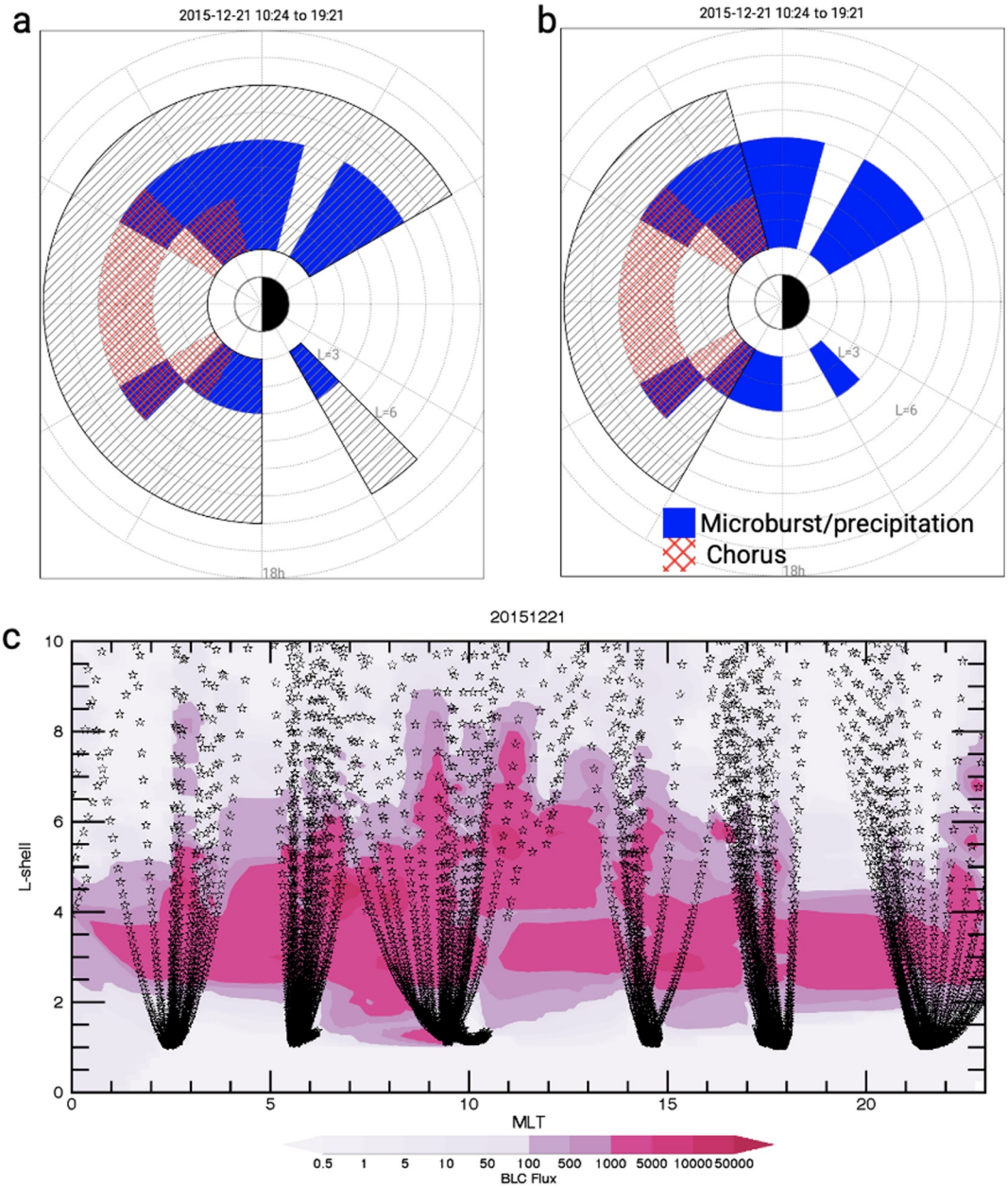

Figure 4. Example (a) upper and (b) lower bounds for an event on 21 December 2015 from 10:24 to 19:21 UT. Upper bounds shown are for Type 1 precipitation. Lower bounds are constrained to the region of overlap between chorus and Type 1 precipitation observations during the ~9 hr event. Note that all *L* values are included. A region is considered continuous if the data gap is within 1 hr in MLT for all MLTs except between 10 and 14 MLT where a 4 hr data gap is accepted due to limitations on Polar Operational Environmental Satellites (POES) observations (c). Panel (c) shows the bounce loss cone flux (#/cm^2/sec) from 10 to 20 UTC on 21 December 2015 derived using methods from Pettit et al. (2021) and then interpolated on MLT—*L* using Delaunay triangulation. The stars indicate measurement locations by the various POES Medium Energy Proton and Electron Detector instruments during the same time period.

this, we interpolate across the 10–14 MLT sector. Figure 4c shows the BLC flux during this event using the method from Pettit et al. (2021), which is consistent with our interpolation method. The stars indicate the orbit location of all the POES satellites during this ~9-hr time window. The contours are BLC flux estimations based on a sophisticated spherical triangulation interpolation method to accurately interpolate unevenly-spaced grid points. It should be clear from Figure 3c that observational data from POES is very limited around the 12 MLT

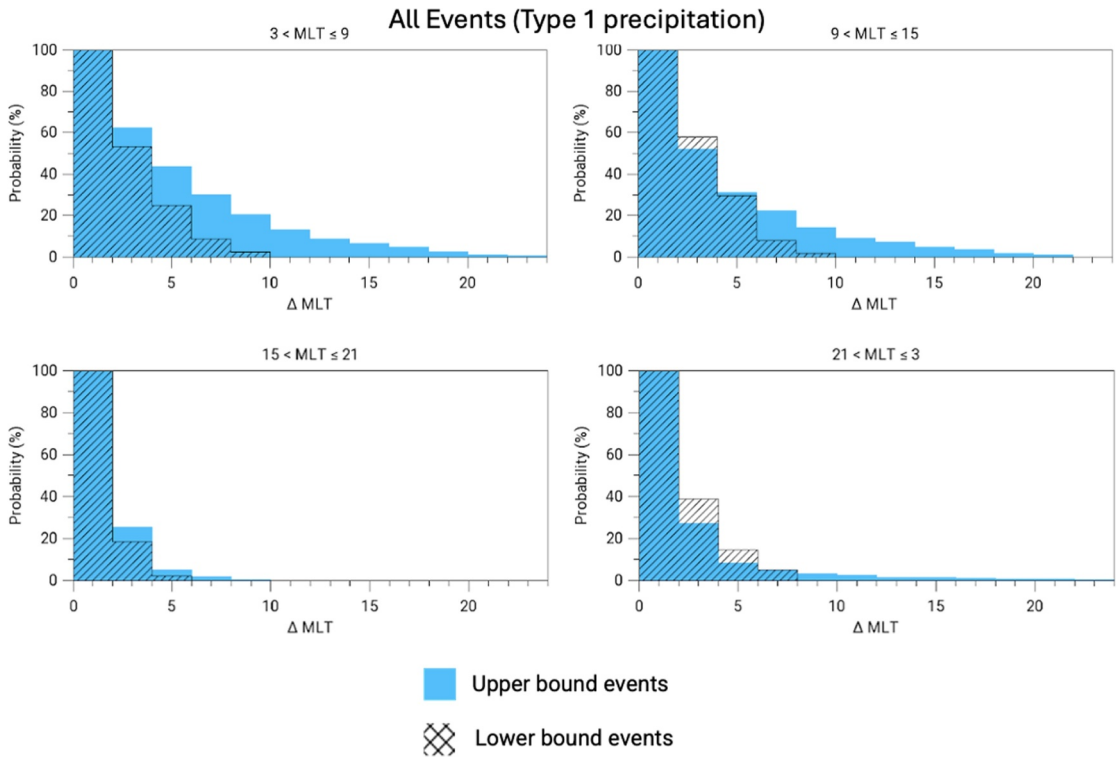

Figure 5. Histograms show the probability of events within or above the bin separated by MLT sector. A total of 894 events were in the 3–9 MLT sector, 378 events were in the 9–15 MLT sector, 287 events were in the 15–21 MLT sector, and 355 events were in the 21–3 MLT sector. The blue bins show the upper bounds and black hashed bins show the lower bounds for Type 1 precipitation. In the 3–9 MLT sector, approximately 36% of upper bound events and approximately 14% of lower bound events are at or above delta MLT of 5.

sector. Despite this, the interpolation method described in Pettit et al. (2021) is able to extrapolate BLC flux estimations across the data gap with reasonable accuracy.

We utilize an automated routine to compute estimates of the upper and lower bounds on the azimuthal extent of the microburst region for both types of precipitation. Figure 2 shows the result of this process. For each event, the corresponding bounds are recorded, along with the average MLT of the region constrained by these bounds, and the geomagnetic conditions during the event (i.e., average AL index). Again, it is important to mention that we are only estimating the MLT extent of the region and therefore all L values are included in each event.

4. Statistical Results and Dependence on Geomagnetic Activity

Figure 5 (Type 1 precipitation) and 6 (Type 2 precipitation) show the statistical results of upper (blue bars) and lower (black hashed bars) bounds for all events, separated by MLT sector (determined by the average MLT for each event). The histograms show the probability of an event being greater than or equal to a given delta MLT value (i.e., 100% of events are at least 1-hr in delta MLT for both upper and lower bound estimates). The majority of events occur in the dawn (3–9) and noon (9–15) MLT sectors, with a total of 894 Type 1 and 63 Type 2 events in the dawn MLT sector and 378 Type 1 and 97 Type 2 events in the noon MLT sector. It should be noted that large events can span multiple MLT sectors. Separating into sectors using the average MLT is to ensure there aren't outlier events outside the typical chorus/microburst region drastically affecting our delta-MLT statistics.

Chorus wave activity has been shown to be closely associated with plasma sheet electron injections during substorms (e.g., R. R. Anderson & Maeda, 1977; Li et al., 2008, 2009; Meredith et al., 2004; Santolik et al., 2010). In this study, we use the average AL index over each ∼9 hr event to analyze how the geomagnetic activity impacts our statistics. AL index has been previously used to study chorus wave properties and occurrence rates (Li et al., 2016; S. Zhang et al., 2021). Microburst occurrence rates have also been found to increase during the recovery phase of geomagnetic storms (Blum, Halford, et al., 2015; Blum, Li, & Denton, 2015; Kurita et al., 2016). Figure 7 shows the statistical results in the same format as Figure 5 but separated out by average AL

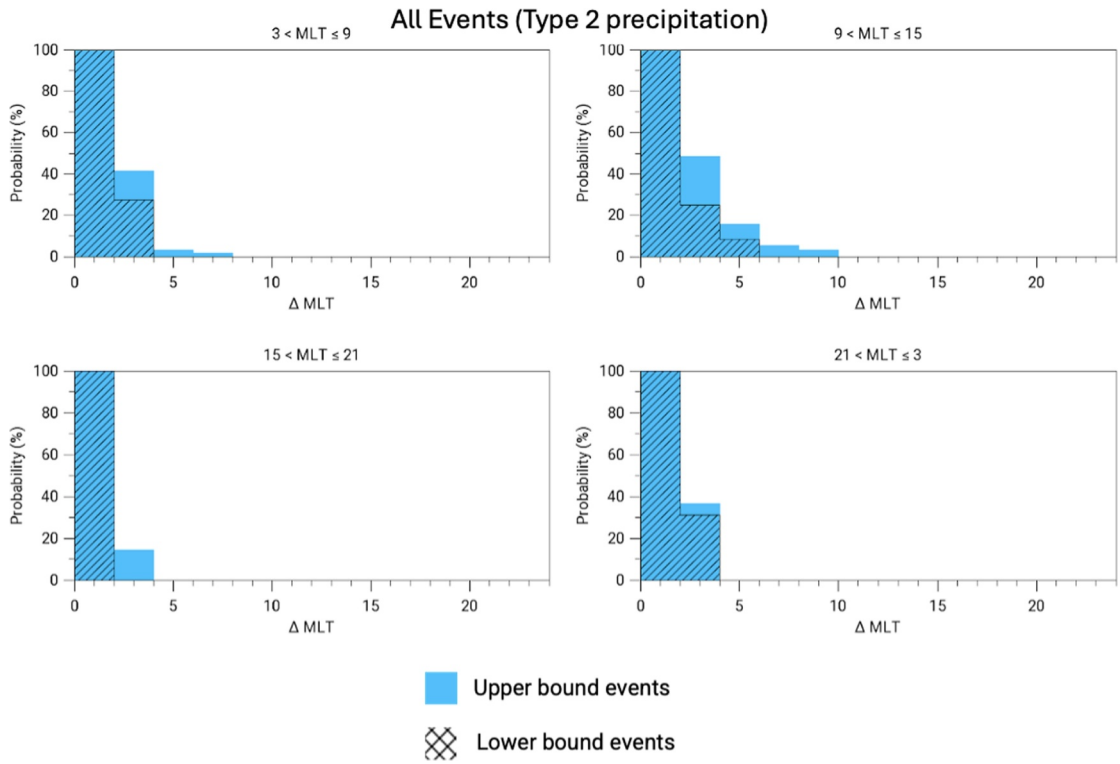

Figure 6. Histograms show the probability of events within or above the bin separated by MLT sector. A total of 63 events were in the 3–9 MLT sector, 97 events were in the 9–15 MLT sector, 14 events were in the 15–21 MLT sector, and 41 events were in the 21–3 MLT sector. The blue bins show the upper bounds and black hashed bins show the lower bounds for Type 2 precipitation. In the 3–9 MLT sector, approximately 3% of upper bound events are at or above delta MLT of 5. In the 9–15 MLT sector approximately 6% of upper bound events are at or above delta MLT of 5.

index over each ∼9 hr event. It is immediately apparent that as geomagnetic activity increases, the microburst region increases in size, especially in the dawn and noon MLT sectors. A similar trend can be observed for Type 2 precipitation (not shown).

In order to determine the relative importance of microburst precipitation as a loss process for outer radiation belt electrons, the mean microburst flux is needed in addition to the size of the precipitation region. Breneman et al. (2017) found this value to be approximately 69 $\left(\text{cm}^2\text{s sr keV}\right)^{-1}$. The associated loss timescale for this mean microburst flux is roughly 10 hr for events with azimuthal extents of 5 ΔMLT, which is comparable to the duration of a single storm. We therefore use ≥5ΔMLT to gauge the significance of a given event. We also attempted to calculate the mean flux for several of our events using the POES BLC precipitation and found that the flux varied by more than a factor of 2 for our lower and upper bounds, and that events occurring in different MLT sectors produced significantly different mean microburst flux estimates (i.e., higher microburst flux was observed in some MLT sectors more than others). This result indicates that we need better constraints on the region size than what is currently possible with the given data set to definitively quantify the importance of this process.

Our statistical results show that for Type 1 precipitation more than 30% of all upper bound events are ≥5 ΔMLT (Figure 5). Specifically, in the dawn sector, for AL indices between −500 and −200 nT, ∼50% of upper bound events are ≥5 ΔMLT and for AL indices less than −500 nT, ∼90% of upper bound events are ≥5 ΔMLT. For Type 2 precipitation (Figure 6), significantly fewer events are ≥5 ΔMLT. This is likely due to the lack of coverage for direct microburst detections; however, there are still a number of events that span multiple MLTs. These results indicate that microburst precipitation is likely a significant loss source of outer radiation belt electrons, but a comprehensive statistical analysis is difficult to do with the current observational data set.

5. Conclusions

Constraining the extent of the microburst-producing chorus region is vital to understanding whether microburst precipitation is a significant loss mechanism for relativistic electrons in the outer radiation belt. This loss has

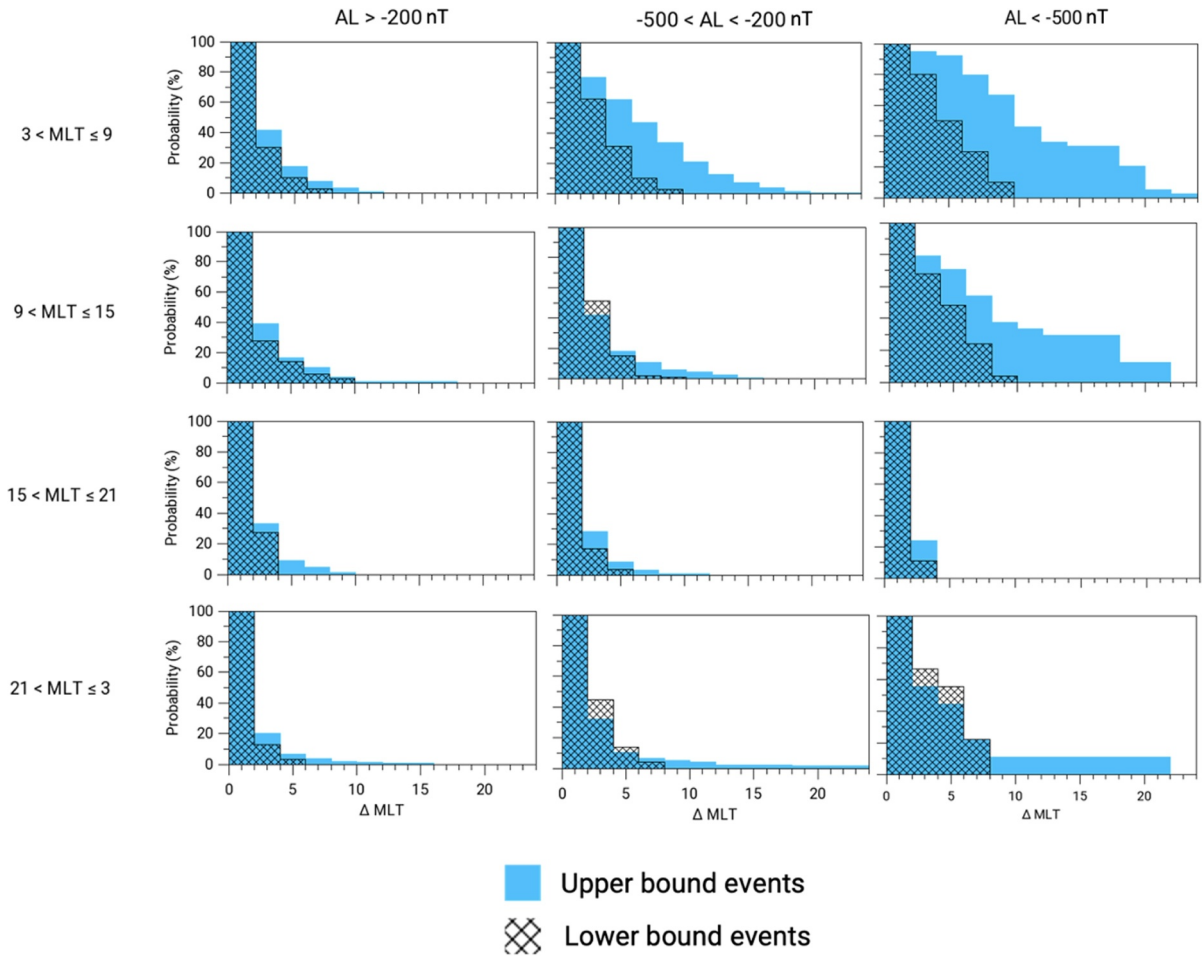

Figure 7. Same format as Figure 5 (Type 1 precipitation) but separated by average AL index during each ~9 hr event. As geomagnetic activity increases, events occur over a wider MLT range. For example, within the 3–9 MLT sector, approximately 55% of upper bound events and approximately 18% of lower bound events are at or above 5 delta MLT when the average AL index is within −500 and −200 nT. Within this same MLT sector, approximately 87% of upper bound events and approximately 30% of lower bound events are at or above 5 delta MLT when the average AL index is below −500 nT. A similar trend is observed in the 9–15 MLT sector.

important implications for magnetosphere-ionosphere coupling and atmospheric composition. We have conducted a statistical analysis of multipoint observations of chorus and microburst precipitation to estimate the azimuthal spatial extent (ΔMLT) of the microburst region. We present upper and lower bounds on the estimated size of the region. The statistics are presented for both combined microburst and POES BLC flux precipitation (Type 1 precipitation) as well as for only direct microburst precipitation (Type 2 precipitation). For Type 1 precipitation, the upper bound represents regions where chorus and microburst and/or POES BLC flux precipitation are observed contemporaneously, along with regions where microburst and/or POES BLC flux precipitation is observed without chorus due to lack of spacecraft coverage. For Type 2 precipitation, the upper bound represents regions where direct microbursts are observed and the lower bound represents regions where both chorus and direct microbursts are observed.

The constraints obtained from this statistical analysis confirm that the region is often large and extended in MLT. The region is shown to expand as geomagnetic activity (based on AL index values) increases, particularly in the dawn and noon MLT sectors, where most events occur. Considerations of the estimated average flux suggest that microbursts can constitute a significant source of electron loss from the outer radiation belt. However, the relative importance of microbursts as a loss process cannot be fully quantified without accurate measurements of the flux of microbursts through a given area over a given amount of time. For example, the use of 9-hr intervals is necessary in order to provide sufficient coverage to estimate the size of the region. However, we know that microburst precipitation is not constant over these timescales, and in fact occurs within the typical 2–3 hr substorm interval. The

current study represents what is currently achievable given the existing observational fleet. However, new missions are required, including imagers and constellation missions with multipoint observations at LEO and wave and particle measurements at varying latitudes and altitudes in order to achieve this spatial resolution with sufficient time resolution on the order of substorm dynamic timescales (Elliott, Breneman, Colpitts, Bortnik, et al., 2022).

Data Availability Statement

Data—Science data of the Van Allen Probes (RBSP) used in this study can be found on the Coordinated Data Analysis Web (CDAWeb) (https://cdaweb.gsfc.nasa.gov/) (EFW data is also available on http://www.space.umn.edu/rbspefw-data/ and EMFISIS on https://emfisis.physics.uiowa.edu/data/index), see Kletzing et al. (2013).

Data—The FIREBIRD II data are available at http://solar.physics.montana.edu/FIREBIRD_II/ and the AC6 data are available at https://rbspgway.jhuapl.edu/ac6. See Klumpar et al. (2015).

Data—Science data of the ERG (Arase) satellite were obtained from the ERG Science Center operated by ISAS/JAXA and ISEE/Nagoya University (https://ergsc.isee.nagoya-u.ac.jp/index.shtml.en), see Miyoshi, Hori, et al. (2018). The present study analyzed PWE OFA L2 power spectrum data v02_02 (Kasahara et al., 2021). PWE WFC L2 electric field spectrum data v00_02 (Kasahara, Kojima, Matsuda, Shoji et al., 2020). PWE WFC L2 magnetic field spectrum data v00_02 (Kasahara, Kojima, Matsuda, Ozaki, et al., 2020). HEP L2 omniflux data v03_01 (Mitani et al., 2018), MGF L2 8 s spin-averaged data v03.04 (Matsuoka, Teramoto, Imajo, et al., 2018), and Orbit L2 v03 data v03 (Miyoshi, Shinohara, & Jun, 2018).

Data—The POES MEPED data is available at the National Centers for Environmental Information (NCEI) at https://www.ngdc.noaa.gov/stp/satellite/poes/dataaccess.html. See Evans and Greer (2004) and Rodger et al. (2010).

Data—BARREL data are available on CDAWeb (https://cdaweb.gsfc.nasa.gov/). Used for this study were the v10 calibrated l2 data products. See Millan et al. (2013).

Software—Figures were made with Autoplot software (https://autoplot.org/).

Acknowledgments
Work at the University of Minnesota and NASA Goddard was supported by the NASA Heliophysics Supporting Research program NNH18ZDA001N-HSR award 80NSSC19K0842. The authors would like to acknowledge Jeremy Faden and the use of Autoplot. JMP acknowledges funding from the NSF Coupling, Energetics and Dynamics of Atmospheric Regions, Grant AGS 1651428 and the NASA Living With a Star program, Grant NNX14AH54G. KAC acknowledges NASA Grant 80NSSC24K0241, Dartmouth College, and the BARREL team.

References

Agapitov, O. V., Blum, L. W., Mozer, F. S., Bonnell, J. W., & Wygant, J. (2017). Chorus whistler wave source scales as determined from multipoint Van Allen Probe measurements. *Geophysical Research Letters*, *44*(6), 2634–2642. https://doi.org/10.1002/2017GL072701

Anderson, B. R., Shekhar, S., Millan, R. M., Crew, A. B., Spence, H. E., Klumpar, D. M., et al. (2017). Spatial scale and duration of one microburst region on 13 August 2015. *Journal of Geophysical Research: Space Physics*, *122*(6), 5949–5964. https://doi.org/10.1002/2016JA023752

Anderson, K. A., & Milton, D. W. (1964). Balloon observations of X rays in the auroral zone: 3. High time resolution studies. *Journal of Geophysical Research*, *69*(21), 4457–4479. https://doi.org/10.1029/JZ069i021p04457

Anderson, R. R., & Maeda, K. (1977). VLF emissions associated with enhanced magnetospheric electrons. *Journal of Geophysical Research*, *82*(1), 135–146. https://doi.org/10.1029/JA082i001p00135

Bingham, S. T., Mouikis, C. G., Kistler, L. M., Boyd, A. J., Paulson, K., Farrugia, C. J., et al. (2018). The outer radiation belt response to the storm time development of seed electrons and chorus wave activity during CME and CIR driven storms. *Journal of Geophysical Research: Space Physics*, *123*, 10139–10157. https://doi.org/10.1029/2018JA025963

Blake, J. B., Looper, M. D., Baker, D. N., Nakamura, R., Klecker, B., & Hovestadt, D. (1996). New high temporal and spatial resolution measurements by SAMPEX of the precipitation of relativistic electrons. *Advances in Space Research*, *18*(8), 171–186. https://doi.org/10.1016/0273-1177(95)00969-8

Blum, L. W., & Breneman, A. W. (2020). Chapter 3 – Observations of radiation belt losses due to cyclotron wave-particle interactions. In *The dynamic loss of Earth's radiation belts*. Elsevier. https://doi.org/10.1016/B978-0-12-813371-2.00003-2

Blum, L. W., Halford, A., Millan, R., Bonnell, J. W., Goldstein, J., Usanova, M., et al. (2015). Observations of coincident EMIC wave activity and duskside energetic electron precipitation on 18-19 January 2013. *Geophysical Research Letters*, *42*(14), 5727–5735. https://doi.org/10.1002/2015GL065245

Blum, L. W., Li, X., & Denton, M. (2015). Rapid MeV electron precipitation as observed by SAMPEX/HILT during high-speed stream-driven storms. *Journal of Geophysical Research: Space Physics*, *120*(5), 3783–3794. https://doi.org/10.1002/2014ja020633

Blum, L. W., Remya, B., Denton, M. H., & Schiller, Q. (2020). Persistent EMIC wave activity across the nightside inner magnetosphere. *Geophysical Research Letters*, *47*(6), e2020GL087009. https://doi.org/10.1029/2020GL087009

Bortnik, J., & Thorne, R. M. (2007). The dual role of ELF/VLF chorus waves in the acceleration and precipitation of radiation belt electrons. *Journal of Atmospheric and Solar-Terrestrial Physics*, *69*(3), 378–386. https://doi.org/10.1016/j.jastp.2006.05.030

Breneman, A. W., Crew, A., Sample, J., Klumpar, D., Johnson, A., Agapitov, O., et al. (2017). Observations directly linking relativistic electron microbursts to whistler mode chorus: Van Allen Probes and FIREBIRD II. *Geophysical Research Letters*, *44*(22), 11–265. https://doi.org/10.1002/2017GL075001

Cantwell, K., & Millan, R. (2024). BARREL observations of microburst events with a slowly-varying component. *Geophysical Research Letters*, *51*(9), e2023GL106277. https://doi.org/10.1029/2023GL106277

Capannolo, L., Li, W., Ma, Q., Qin, M., Shen, X.-C., Angelopoulos, V., et al. (2023). Electron precipitation observed by ELFIN using proton precipitation as a proxy for electromagnetic ion cyclotron (EMIC) waves. *Geophysical Research Letters*, *50*(21), e2023GL103519. https://doi.org/10.1029/2023GL103519

Capannolo, L., Li, W., Ma, Q., Shen, X. C., Zhang, X. J., Redmon, R. J., et al. (2019). Energetic electron precipitation: Multievent analysis of its spatial extent during EMIC wave activity. *Journal of Geophysical Research: Space Physics*, *124*(4), 2466–2483. https://doi.org/10.1029/2018ja026291

Capannolo, L., Li, W., Ma, Q., Zhang, X.-J., Redmon, R. J., Rodriguez, J. V., et al. (2018). Understanding the driver of energetic electron precipitation using coordinated multisatellite measurements. *Geophysical Research Letters*, *45*(14), 6755–6765. https://doi.org/10.1029/2018GL078604

Capannolo, L., Li, W., Millan, R., Smith, D., Sivadas, N., Sample, J., & Shekhar, S. (2022). Relativistic electron precipitation near midnight: Drivers, distribution, and properties. *Journal of Geophysical Research: Space Physics*, *127*(1), e2021JA030111. https://doi.org/10.1029/2021ja030111

Capannolo, L., Li, W., Spence, H., Johnson, A. T., Shumko, M., Sample, J., & Klumpar, D. (2021). Energetic electron precipitation observed by FIREBIRD-II potentially driven by EMIC waves: Location, extent, and energy range from a multievent analysis. *Geophysical Research Letters*, *48*(5), e2020GL091564. https://doi.org/10.1029/2020GL091564

Carson, B. R., Rodger, C. J., & Clilverd, M. A. (2012). POES satellite observations of EMIC-wave driven relativistic electron precipitation during 1998–2010. *Journal of Geophysical Research*, *118*(1), 232–243. https://doi.org/10.1029/2012JA017998

Chen, L., Zhang, X.-J., Artemyev, A., Angelopoulos, V., Tsai, E., Wilkins, C., & Horne, R. B. (2022). Ducted chorus waves cause sub-relativistic and relativistic electron microbursts. *Geophysical Research Letters*, *49*(5), e2021GL097559. https://doi.org/10.1029/2021GL097559

Chen, L., Zhang, X.-J., Artemyev, A., Zheng, L., Zhiyang, X., Breneman, A. W., & Horne, R. B. (2021). Electron microburst induced by nonducted chorus waves. *Frontiers in Astronomy and Space Sciences*, *8*, 745927. https://doi.org/10.3389/fspas.2021.745927

Colpitts, C., Miyoshi, Y., Kasahara, Y., Delzanno, G. L., Wygant, J. R., Cattell, C. A., et al. (2020). First direct observations of propagation of discrete chorus elements from the equatorial source to higher latitudes, using the Van Allen Probes and Arase satellites. *Journal of Geophysical Research: Space Physics*, *125*(10), e2020JA028315. https://doi.org/10.1029/2020JA028315

Crew, A. B., Spence, H. E., Blake, J. B., Klumpar, D. M., Larsen, B. A., O'Brien, T. P., et al. (2016). First multipoint in situ observations of electron microbursts: Initial results from the NSF FIREBIRD II mission. *Journal of Geophysical Research: Space Physics*, *121*(6), 5272–5283. https://doi.org/10.1002/2016JA022485

Douma, E., Rodger, C., Blum, L., O'Brien, T., Clilverd, M., & Blake, J. (2019). Characteristics of relativistic microburst intensity from SAMPEX observations. *Journal of Geophysical Research: Space Physics*, *124*(7), 5627–5640. https://doi.org/10.1029/2019JA026757

Douma, E., Rodger, C. J., Blum, L. W., & Clilverd, M. A. (2017). Occurrence characteristics of relativistic electron microbursts from SAMPEX observations. *Journal of Geophysical Research: Space Physics*, *122*(8), 8096–8107. https://doi.org/10.1002/2017JA024067

Drozdov, A. Y., Aseev, N., Effenberger, F., Turner, D. L., Saikin, A., & Shprits, Y. (2019). Storm time depletions of multi-MeV radiation belt electrons observed at different pitch angles. *Journal of Geophysical Research: Space Physics*, *124*(11), 8943–8953. https://doi.org/10.1029/2019JA027332

Drozdov, A. Y., Usanova, M. E., Hudson, M. K., Allison, H. J., & Shprits, Y. (2020). The role of hiss, chorus, and EMIC waves in the modeling of the dynamics of the multi-MeV radiation belt electrons. *Journal of Geophysical Research: Space Physics*, *125*(9), e2020JA028282. https://doi.org/10.1029/2020ja028282

Elliott, S. S., Breneman, A., Colpitts, C., Bortnik, J., Jaynes, A., Halford, A., et al. (2022). Understanding the properties, wave drivers, and impacts of electron microburst precipitation: Current understanding and critical knowledge gaps. *Frontiers in Astronomy and Space Sciences*, *9*, 1062422. https://doi.org/10.3389/fspac.2022.1062422

Elliott, S. S., Breneman, A. W., Colpitts, C., Pettit, J. M., Cattell, C. A., Halford, A. J., et al. (2022). Quantifying the size and duration of a microburst-producing chorus region on 5 December 2017. *Geophysical Research Letters*, *49*(15), e2022GL099655. https://doi.org/10.1029/2022GL099655

Engebretson, M. J., Lessard, M. R., Bortnik, J., Green, J. C., Horne, R. B., Detrick, D. L., et al. (2008). Pc1–Pc2 waves and energetic particle precipitation during and after magnetic storms: Superposed epoch analysis and case studies. *Journal of Geophysical Research*, *113*(A1), A01211. https://doi.org/10.1029/2007JA012362

Evans, D. S., & Greer, M. S. (2004). *Polar orbiting environmental satellite space environment monitor-2: Instrument descriptions and archive data documentation, NOAA Tech. Mem., version 1.4*. Space Weather Prediction Center.

Hartley, D. P., Chen, Y., Kletzing, C. A., Denton, M. H., & Kurth, W. S. (2015). Applying the cold plasma dispersion relation to whistler mode chorus waves: EMFISIS wave measurements from the Van Allen Probes. *Journal of Geophysical Research: Space Physics*, *120*(2), 1144–1152. https://doi.org/10.1002/2014JA020808

Hartley, D. P., Kletzing, C. A., Chen, L., Horne, R. B., & Santolík, O. (2019). Van Allen Probes observations of chorus wave vector orientations: Implications for the chorus-to-hiss mechanism. *Geophysical Research Letters*, *46*(5), 2337–2346. https://doi.org/10.1029/2019GL082111

Hartley, D. P., Kletzing, C. A., Kurth, W. S., Bounds, S. R., Averkamp, T. F., Hospodarsky, G. B., et al. (2016). Using the cold plasma dispersion relation and whistler mode waves to quantify the antenna sheath impedance of the Van Allen Probes EFW instrument. *Journal of Geophysical Research: Space Physics*, *121*(5), 4590–4606. https://doi.org/10.1002/2016JA022501

Horne, R. B., Glauert, S. A., & Thorne, R. M. (2003). Resonant diffusion of radiation belt electrons by whistler-mode chorus. *Geophysical Research Letters*, *30*(9), 1493. https://doi.org/10.1029/2003GL016963

Huang, C.-S. (2005). Variations of polar cap index in response to solar wind changes and magnetospheric substorms. *Journal of Geophysical Research*, *110*(A1), A01203. https://doi.org/10.1029/2004JA010616

Imhof, W. L., & Nightingale, R. W. (1992). Relativistic electron enhancements observed over a range of L shells trapped at high altitudes and precipitating at low altitudes into the atmosphere. *Journal of Geophysical Research*, *97*(A5), 6397–6403. https://doi.org/10.1029/92JA0022

Johnson, A. T., Shumko, M., Griffith, B., Klumpar, D. M., Sample, J., Springer, L., et al. (2020). The FIREBIRD-II CubeSat mission: Focused investigations of relativistic electron burst intensity, range, and dynamics. *Review of Scientific Instruments*, *91*(3), 034503. https://doi.org/10.1063/1.5137905

Kanekal, S., & Miyoshi, Y. (2021). Dynamics of the terrestrial radiation belts: A review of recent results during the VarSITI (variability of the sun and its terrestrial impact) era, 2014–2018. *Progress in Earth and Planetary Science*, *8*(1), 35. https://doi.org/10.1186/s40645-021-00413-y

Kang, N., Artemyev, A. V., Bortnik, J., Zhang, X.-J., & Angelopoulos, V. (2024). The principal role of chorus ducting for night-side relativistic electron precipitation. *Geophysical Research Letters*, *51*(17), e2024GL110365. https://doi.org/10.1029/2024GL110365

Kasaba, Y., Ishisaka, K., Kasahara, Y., Imachi, T., Yagitani, S., Kojima, H., et al. (2017). Wire probe antenna (WPT) and electric field detector (EFD) of plasma wave experiment (PWE) aboard the Arase satellite: Specifications and initial evaluation results. *Earth Planets and Space*, *69*(1), 174. https://doi.org/10.1186/s40623-017-0760-x

Kasahara, Y., Kasaba, Y., Kojima, H., Yagitani, S., Ishisaka, K., Kumamoto, A., et al. (2018). The plasma wave experiment (PWE) on board the Arase (ERG) satellite. *Earth Planets and Space*, *70*(1), 86. https://doi.org/10.1186/s40623-018-0842-4

Kasahara, Y., Kojima, H., Matsuda, S., Ozaki, M., Yagitani, S., Shoji, M., et al. (2020). The PWE/WFC instrument level-2 magnetic field spectrum data of Exploration of energization and Radiation in Geospace (ERG) Arase satellite. https://doi.org/10.34515/DATA.ERG-09003

Kasahara, Y., Kojima, H., Matsuda, S., Ozaki, M., Yagitani, S., Shoji, M., et al. (2021). The PWE/OFA instrument level-2 spectral matrix data of Exploration of energization and Radiation in Geospace (ERG) Arase satellite. https://doi.org/10.34515/DATA.ERG-08001

Kasahara, Y., Kojima, H., Matsuda, S., Shoji, M., Nakamura, S., Kitahara, M., et al. (2020). The PWE/WFC instrument level-2 electric field spectrum data of Exploration of energization and Radiation in Geospace (ERG) Arase satellite. https://doi.org/10.34515/DATA.ERG-09002

Kersten, K., Cattell, C. A., Breneman, A., Goetz, K., Kellogg, P. J., Wygant, J. R., et al. (2011). Observation of relativistic electron microbursts in conjunction with intense radiation belt whistler-mode waves. *Geophysical Research Letters*, *38*(8), L08107. https://doi.org/10.1029/2011GL046810

Kletzing, C., Kurth, W. S., Acuna, M., MacDowall, R. J., Torbert, R. B., Averkamp, T., et al. (2013). The electric and magnetic field instrument suite and integrated science (EMFISIS) on RBSP. *Space Science Reviews*, *179*(1–4), 127–181. https://doi.org/10.1007/s11214-013-9993-6

Klumpar, D., Springer, L., Mosleh, E., Mashburn, K., Berardinelli, S., Gunderson, A., et al. (2015). Flight system technologies enabling the twin-CubeSat FIREBIRD-II scientific mission. In *Proceedings of the 29th annual AIAA/USU conference on small satellites*.

Kurita, S., Miyoshi, Y., Blake, B., Reeves, G., & Kletzing, C. (2016). Relativistic electron microbursts and variations in trapped MeV electron fluxes during the 8-9 October 2012 storm: SAMPEX and Van Allen Probes observations. *Geophysical Research Letters*, *43*(7), 3017–3025. https://doi.org/10.1029/2016GL068260

Li, W., Mourenas, D., Artemyev, A. V., Agapitov, O. V., Bortnik, J., Albert, J. M., et al. (2014). Evidence of stronger pitch angle scattering loss caused by oblique whistler-mode waves as compared with quasi-parallel waves. *Geophysical Research Letters*, *41*(17), 6063–6070. https://doi.org/10.1002/2014GL061260

Li, W., Ni, B., Thorne, R. M., Bortnik, J., Green, J. C., Kletzing, C. A., et al. (2013). Constructing the global distribution of chorus wave intensity using measurements of electrons by the POES satellites and waves by the Van Allen Probes. *Geophysical Research Letters*, *40*(17), 4526–4532. https://doi.org/10.1002/grl.50920

Li, W., Santolik, O., Bortnik, J., Thorne, R. M., Kletzing, C. A., Kurth, W. S., & Hospodarsky, G. B. (2016). New chorus wave properties near the equator from Van Allen Probes wave observations. *Geophysical Research Letters*, *43*(10), 4725–4735. https://doi.org/10.1002/2016GL068780

Li, W., Thorne, R. M., Angelopoulos, V., Bonnell, J. W., McFadden, J. P., Carlson, C. W., et al. (2009). Evaluation of whistler-mode chorus intensification on the nightside during an injection event observed on the THEMIS spacecraft. *Journal of Geophysical Research*, *114*(A1), A00C14. https://doi.org/10.1029/2008JA013554

Li, W., Thorne, R. M., Meredith, N. P., Horne, R. B., Bortnik, J., Shprits, Y. Y., & Ni, B. (2008). Evaluation of whistler mode chorus amplification during an injection event observed on CRRES. *Journal of Geophysical Research*, *113*(A9), A09210. https://doi.org/10.1029/2008JA013129

Lorentzen, K. R., Blake, J. B., Inan, U. S., & Bortnik, J. (2001). Observations of relativistic electron microbursts in association with VLF chorus. *Journal of Geophysical Research*, *106*(A4), 6017–6027. https://doi.org/10.1029/2000JA003018

Lorentzen, K. R., Looper, M. D., & Blake, J. B. (2001). Relativistic electron microbursts during the GEM storms. *Geophysical Research Letters*, *28*(13), 2573–2576. https://doi.org/10.1029/2001GL012926

Ma, Q., Connor, H. K., Zhang, X.-J., Li, W., Shen, X.-C., Gillespie, D., et al. (2020). Global survey of plasma sheet electron precipitation due to whistler mode chorus waves in Earth's magnetosphere. *Geophysical Research Letters*, *47*(15), e2020GL088798. https://doi.org/10.1029/2020GL088798

Marshall, R. A., & Cully, C. M. (2020). Atmospheric effects and signatures of high-energy electron precipitation. *The Dynamic Loss of Earth's Radiation Belts*, 199–255. https://doi.org/10.1016/B978-0-12-813371-2.00007-X

Matsuda, S., Kasahara, Y., Kojima, H., Kasaba, Y., Yagitani, S., Ozaki, M., et al. (2018). Onboard software of plasma wave experiment aboard Arase: Instrument management and signal processing of waveform capture/onboard frequency analyzer. *Earth Planets and Space*, *70*(1), 75. https://doi.org/10.1186/s40623-018-0838-0

Matsuoka, A., Teramoto, M., Imajo, S., Kurita, S., Miyoshi, Y., & Shinohara, I. (2018). The MGF instrument level-2 spin-averaged magnetic field data of Exploration of energization and Radiation in Geospace (ERG) Arase satellite. https://doi.org/10.34515/DATA.ERG-06001

Matsuoka, A., Teramoto, M., Nomura, R., Nosé, M., Fujimoto, A., Tanaka, Y., et al. (2018). The ARASE (ERG) magnetic field investigation. *Earth Planets and Space*, *70*(1), 43. https://doi.org/10.1186/s40623-018-0800-1

Mauk, B. H., Fox, N. J., Kanekal, S. G., Kessel, R. L., Sibeck, D. G., & Ukhorskiy, A. (2013). Science objectives and rationale for the radiation belt storm probes mission. *Space Science Reviews*, *179*(1–4), 3–27. https://doi.org/10.1007/s11214-012-9908-y

Meredith, N. P., Horne, R. B., Thorne, R. M., Summers, D., & Anderson, R. R. (2004). Substorm dependence of plasmaspheric hiss. *Journal of Geophysical Research*, *109*(A6), A06209. https://doi.org/10.1029/2004JA010387

Millan, R. M., Lin, R. P., Smith, D. M., Lorentzen, K. R., & McCarthy, M. P. (2002). X-ray observations of MeV electron precipitation with a balloon-borne germanium spectrometer. *Geophysical Research Letters*, *29*(24), 47-1–47-4. https://doi.org/10.1029/2002GL015922

Millan, R. M., McCarthy, M. P., Sample, J. G., Smith, D. M., Thompson, L. D., McGaw, D. G., et al. (2013). The balloon array for RBSP relativistic electron losses (BARREL). *Space Science Reviews*, *179*(1–4), 503–530. https://doi.org/10.1007/s11214-013-9971-z

Millan, R. M., & Thorne, R. M. (2007). Review of radiation belt relativistic electron losses. *Journal of Atmospheric and Solar-Terrestrial Physics*, *69*(3), 362–377. https://doi.org/10.1016/j.jastp.2006.06.019

Mitani, T., Takashima, T., Kasahara, S., Miyake, W., & Hirahara, M. (2018). High-energy electron experiments (HEP) aboard the ERG (Arase) satellite. *Earth Planets and Space*, *70*(1), 77. https://doi.org/10.1186/s40623-018-0853-1

Miyoshi, Y., Hori, T., Shoji, M., Teramoto, M., Chang, T.-F., Segawa, T., et al. (2018). The ERG Science Center. *Earth Planets and Space*, *70*(1), 96. https://doi.org/10.1186/s40623-018-0867-8

Miyoshi, Y., Hosokawa, K., Kurita, S., Oyama, S. I., Ogawa, Y., Saito, S., et al. (2021). Penetration of MeV electrons into the mesosphere accompanying pulsating aurorae. *Scientific Reports*, *11*(1), 13724. https://doi.org/10.1038/s41598-021-92611-3

Miyoshi, Y., Oyama, S., Saito, S., Kurita, S., Fujiwara, H., Kataoka, R., et al. (2015). Energetic electron precipitation associated with pulsating aurora: EISCAT and Van Allen Probe observations. *Journal of Geophysical Research: Space Physics*, *120*(4), 2754–2766. https://doi.org/10.1002/2014JA020690

Miyoshi, Y., Saito, S., Kurita, S., Asamura, K., Hosokawa, K., Sakanoi, T., et al. (2020). Relativistic electron microbursts as high energy tail of pulsating aurora electrons. *Geophysical Research Letters*, *47*(21), e2020GL090360. https://doi.org/10.1029/2020GL090360

Miyoshi, Y., Shinohara, I., & Jun, C.-W. (2018). The level-2 orbit data of exploration of energization and radiation in geospace (ERG) Arase satellite. https://doi.org/10.34515/DATA.ERG-12000

Miyoshi, Y., Shinohara, I., Takashima, T., Asamura, K., Higashio, N., Mitani, T., et al. (2018). Geospace exploration project ERG. *Earth Planets and Space*, *70*(1), 101. https://doi.org/10.1186/s40623-018-0862-0

Mozer, F. S., Agapitov, O. V., Blake, J. B., & Vasko, I. Y. (2018). Simultaneous observations of lower band chorus emissions at the equator and microburst precipitating electrons in the ionosphere. *Geophysical Research Letters*, *45*(2), 511–516. https://doi.org/10.1002/2017GL076120

Nakamura, R., Isowa, M., Kamide, Y., Baker, D. N., Blake, J. B., & Looper, M. (2000). SAMPEX observations of precipitation bursts in the outer radiation belt. *Journal of Geophysical Research*, *105*(A7), 15875–15885. https://doi.org/10.1029/2000JA900018

Namekawa, T., Mitani, T., Asamura, K., Miyoshi, Y., Hosokawa, K., Lessard, M., et al. (2023). Simultaneous precipitation of sub-relativistic electron microburst and pulsating aurora electrons. *Geophysical Research Letters*, *50*(24), e2023GL104001. https://doi.org/10.1029/2023GL104001

O'Brien, T. P., Looper, M. D., & Blake, J. B. (2004). Quantification of relativistic electron microburst losses during the GEM storms. *Geophysical Research Letters*, *31*(4), L04802. https://doi.org/10.1029/2003GL018621

O'Brien, T. P., Lorentzen, K. R., Mann, I. R., Meredith, N. P., Blake, J. B., Fennell, J. F., et al. (2003). Energization of relativistic electrons in the presence of ULF power and MeV microbursts: Evidence for dual ULF and VLF acceleration. *Journal of Geophysical Research*, *108*(A8), 1329. https://doi.org/10.1029/2002JA009784

Ozaki, M., Yagitani, S., Kasahara, Y., Kojima, H., Kasaba, Y., Kumamoto, A., et al. (2018). Magnetic search coil (MSC) of plasma wave experiment (PWE) aboard the Arase (ERG) satellite. *Earth Planets and Space*, *70*(1), 76. https://doi.org/10.1186/s40623-018-0837-1

Pettit, J. M., Elliott, S., Randall, C., Halford, A., Jaynes, A., & Garcia-Sage, K. (2023). Investigation of the drivers and atmospheric impacts of energetic electron precipitation. *Frontiers in Astronomy and Space Sciences*, *10*, 1162564. https://doi.org/10.3389/fspas.2023.1162564

Pettit, J. M., Randall, C. E., Peck, E. D., & Harvey, V. L. (2021). A new MEPED-based precipitating electron data set. *Journal of Geophysical Research: Space Physics*, *126*(12), e2021JA029667. https://doi.org/10.1029/2021JA029667

Qin, M., Hudson, M., Millan, R., Woodger, L., & Shen, X. (2020). Statistical dependence of EMIC wave scattering on wave and plasma parameters. *Journal of Geophysical Research: Space Physics*, *125*(4), e2020JA027772. https://doi.org/10.1029/2020JA027772

Ripoll, J.-F., Claudepierre, S. G., Ukhorskiy, A. Y., Colpitts, C., Li, X., Fennell, J., & Crabtree, C. (2020). Particle dynamics in the Earth's radiation belts: Review of current research and open questions. *Journal of Geophysical Research: Space Physics*, *125*(5), e2019JA026735. https://doi.org/10.1029/2019JA026735

Rodger, C. J., Cliverd, M. A., Green, J. C., & Lam, M. M. (2010). Use of POES SEM-2 observations to examine radiation belt dynamics and energetic electron precipitation into the atmosphere. *Journal of Geophysical Research*, *115*(A4), A04202. https://doi.org/10.1029/2008JA014023

Saito, S., Miyoshi, Y., & Seki, K. (2012). Relativistic electron microbursts associated with whistler chorus rising tone elements: GEMSIS-RBW simulations. *Journal of Geophysical Research*, *117*(A10), A10206. https://doi.org/10.1029/2012JA018020

Santolik, O., Gurnett, D. A., Pickett, J. S., Grimald, S., Decreau, P. M. E., Parrot, M., et al. (2010). Wave-particle interactions in the equatorial source region of whistler-mode emissions. *Journal of Geophysical Research*, *115*(A8), A00F16. https://doi.org/10.1029/2009JA015218

Santolík, O., Pickett, J. S., Gurnett, D. A., & Storey, L. R. O. (2002). Magnetic component of narrow-band ion cyclotron waves in the auroral zone. *Journal of Geophysical Research*, *107*(A12), 1444. https://doi.org/10.1029/2001JA000146

Selesnick, R. S., Tu, W., Yando, K. B., Millan, R. M., & Redmon, R. J. (2020). POES/MEPED angular response functions and the precipitating radiation belt electron flux. *Journal of Geophysical Research: Space Physics*, *125*(9), e2020JA028240. https://doi.org/10.1029/2020JA028240

Seppälä, A., Douma, E., Rodger, C. J., Verronen, P. T., Clilverd, M. A., & Bortnik, J. (2018). Relativistic electron microburst events: Modeling the atmospheric impact. *Geophysical Research Letters*, *45*(2), 1141–1147. https://doi.org/10.1002/2017GL075949

Shekhar, S., Millan, R., & Smith, D. (2017). A statistical study of the spatial extent of relativistic electron precipitation with polar orbiting environmental satellites. *Journal of Geophysical Research: Space Physics*, *122*(11), 11274–11284. https://doi.org/10.1002/2017JA024716

Shekhar, S., Millan, R. M., & Hudson, M. K. (2018). A statistical study of spatial variation of relativistic electron precipitation energy spectra with Polar Operational Environmental Satellites. *Journal of Geophysical Research: Space Physics*, *123*(5), 3349–3359. https://doi.org/10.1002/2017JA025041

Shprits, Y. Y., Kellerman, A., Aseev, N., Drozdov, A. Y., & Michaelis, I. (2017). Multi-MeV electron loss in the heart of the radiation belts. *Geophysical Research Letters*, *44*(3), 1204–1209. https://doi.org/10.1002/2016GL072258

Shumko, M., Johnson, A. T., Sample, J. G., Griffith, B. A., Turner, D. L., O'Brien, T. P., et al. (2020). Electron microburst size distribution derived with AeroCube-6. *Journal of Geophysical Research: Space Physics*, *125*(3), e2019JA027651. https://doi.org/10.1029/2019JA027651

Shumko, M., Miyoshi, Y., Blum, L. W., Halford, A. J., Breneman, A. W., Johnson, A. T., et al. (2023). Observation of an electron microburst with an inverse time-of-flight energy dispersion. *Geophysical Research Letters*, *50*(15), e2023GL104804. https://doi.org/10.1029/2023GL104804

Spence, H. E., Blake, J. B., Crew, A. B., Driscoll, S., Klumpar, D. M., Larsen, B. A., et al. (2012). Focusing on size and energy dependence of electron microbursts from the Van Allen radiation belts. *Space Weather*, *10*(11), S11004. https://doi.org/10.1029/2012SW000869

Thorne, R. M. (2010). Radiation belt dynamics: The importance of wave particle interactions. *Geophysical Research Letters*, *37*(22), L22107. https://doi.org/10.1029/2010GL044990

Thorne, R. M., O'Brien, T. P., Shprits, Y. Y., Summers, D., & Horne, R. B. (2005). Timescale for MeV electron microburst loss during geomagnetic storms. *Journal of Geophysical Research*, *110*(A9), A09202. https://doi.org/10.1029/2004JA010882

Troyer, R. N., Jaynes, A. N., Hartley, D. P., Meredith, N. P., Hua, M., & Bortnik, J. (2024). Substorm driven chorus waves: Decay timescales and implications for pulsating aurora. *Journal of Geophysical Research: Space Physics*, *129*(1), e2023JA031883. https://doi.org/10.1029/2023ja031883

Tsurutani, B. T., Lakhina, G. S., & Verkhoglyadova, O. P. (2013). Energetic electron (>10 keV) microburst precipitation, ~5–15 s X-ray pulsations, chorus, and wave-particle interactions: A review. *Journal of Geophysical Research: Space Physics*, *118*(5), 2296–2312. https://doi.org/10.1002/jgra.50264

Woodger, L. A., Halford, A. J., Millan, R. M., McCarthy, M. P., Smith, D. M., Bowers, G. S., et al. (2015). A summary of the BARREL campaigns: Technique for studying electron precipitation. *Journal of Geophysical Research: Space Physics*, *120*(6), 4922–4935. https://doi.org/10.1002/2014ja020874

Woodger, L. A., Millan, R. M., Li, Z., & Sample, J. G. (2018). Impact of background magnetic field for EMIC wave-driven electron precipitation. *Journal of Geophysical Research: Space Physics*, *123*(10), 8518–8532. https://doi.org/10.1029/2018JA025315

Xiang, Z., Tu, W., Li, X., Ni, B., Morley, S. K., & Baker, D. N. (2017). Understanding the mechanisms of radiation belt dropouts observed by Van Allen Probes. *Journal of Geophysical Research: Space Physics*, *122*(10), 9858–9879. https://doi.org/10.1002/2017JA024487

Yuan, Z., Liu, K., Yu, X., Yao, F., Huang, S., Wang, D., & Ouyang, Z. (2018). Precipitation of radiation belt electrons by EMIC waves with conjugated observations of NOAA and Van Allen satellites. *Geophysical Research Letters*, *45*(23), 12694–12702. https://doi.org/10.1029/2018GL080481

Zhang, S., Rae, I. J., Watt, C. E. J., Degeling, A. W., Tian, A., Shi, Q., et al. (2021). Determining the global scale size of chorus waves in the magnetosphere. *Journal of Geophysical Research: Space Physics*, *126*(11), e2021JA029569. https://doi.org/10.1029/2021JA029569

Zhang, X.-J., Angelopoulos, V., Mourenas, D., Artemyev, A., Tsai, E., & Wilkins, C. (2022). Characteristics of electron microburst precipitation based on high-resolution ELFIN measurements. *Journal of Geophysical Research: Space Physics*, *127*(5), e2022JA030509. https://doi.org/10.1029/2022JA030509

Zhang, X.-J., Li, W., Ma, Q., Thorne, R. M., Angelopoulos, V., Bortnik, J., et al. (2016). Direct evidence for EMIC wave scattering of relativistic electrons in space. *Journal of Geophysics Research: Space Physics*, *121*(7), 6620–6631. https://doi.org/10.1002/2016JA022521